

New sperm whale remains from the late Miocene  
of the North Sea and a revised family attribution  
for the small crown physeteroid  
*Thalassocetus* Abel, 1905

Apolline ALFSEN, Mark BOSSELAERS & Olivier LAMBERT



DIRECTEURS DE LA PUBLICATION / PUBLICATION DIRECTORS :  
Bruno David, Président du Muséum national d'Histoire naturelle  
Étienne Ghys, Secrétaire perpétuel de l'Académie des sciences

RÉDACTEURS EN CHEF / EDITORS-IN-CHIEF: Michel Laurin (CNRS), Philippe Taquet (Académie des sciences)

ASSISTANTE DE RÉDACTION / ASSISTANT EDITOR: Adenise Lopes (Académie des sciences; [cr-palevol@academie-sciences.fr](mailto:cr-palevol@academie-sciences.fr))

MISE EN PAGE / PAGE LAYOUT: Audrina Neveu (Muséum national d'Histoire naturelle; [audrina.neveu@mnhn.fr](mailto:audrina.neveu@mnhn.fr))

RÉVISIONS LINGUISTIQUES DES TEXTES ANGLAIS / ENGLISH LANGUAGE REVISIONS: Kevin Padian (University of California at Berkeley)

RÉDACTEURS ASSOCIÉS / ASSOCIATE EDITORS (\*, *took charge of the editorial process of the article/a pris en charge le suivi éditorial de l'article*):

Micropaléontologie/*Micropalaeontology*

Maria Rose Petrizzo (Università di Milano, Milano)

Paléobotanique/*Palaeobotany*

Cyrille Prestianni (Royal Belgian Institute of Natural Sciences, Brussels)

Métazoaires/*Metazoa*

Annalisa Ferretti (Università di Modena e Reggio Emilia, Modena)

Paléochthyologie/*Palaeoichthyology*

Philippe Janvier (Muséum national d'Histoire naturelle, Académie des sciences, Paris)

Amniotes du Mésozoïque/*Mesozoic amniotes*

Hans-Dieter Sues (Smithsonian National Museum of Natural History, Washington)

Tortues/*Turtles*

Juliana Sterli (CONICET, Museo Paleontológico Egidio Feruglio, Trelew)

Lépidosauromorphes/*Lepidosauromorphs*

Hussam Zaher (Universidade de São Paulo)

Oiseaux/*Birds*

Eric Buffetaut (CNRS, École Normale Supérieure, Paris)

Paléomammalogie (mammifères de moyenne et grande taille)/*Palaeomammalogy (large and mid-sized mammals)*

**Lorenzo Rook\*** (Università degli Studi di Firenze, Firenze)

Paléomammalogie (petits mammifères sauf Euarchontoglires)/*Palaeomammalogy (small mammals except for Euarchontoglires)*

Robert Asher (Cambridge University, Cambridge)

Paléomammalogie (Euarchontoglires)/*Palaeomammalogy (Euarchontoglires)*

K. Christopher Beard (University of Kansas, Lawrence)

Paléoanthropologie/*Palaeoanthropology*

Roberto Macchiarelli (Université de Poitiers, Poitiers)

Archéologie préhistorique/*Prehistoric archaeology*

Marcel Otte (Université de Liège, Liège)

RÉFÉRÉS / REVIEWERS: <https://sciencepress.mnhn.fr/fr/periodiques/comptes-rendus-palevol/referes-du-journal>

COUVERTURE / COVER:

Made from the Figures of the article.

*Comptes Rendus Palevol* est indexé dans / *Comptes Rendus Palevol is indexed by:*

- Cambridge Scientific Abstracts
- Current Contents® Physical
- Chemical, and Earth Sciences®
- ISI Alerting Services®
- Geoabstracts, Geobase, Georef, Inspec, Pascal
- Science Citation Index®, Science Citation Index Expanded®
- Scopus®.

Les articles ainsi que les nouveautés nomenclaturales publiés dans *Comptes Rendus Palevol* sont référencés par /  
*Articles and nomenclatural novelties published in Comptes Rendus Palevol are registered on:*

- ZooBank® (<http://zoobank.org>)

*Comptes Rendus Palevol* est une revue en flux continu publiée par les Publications scientifiques du Muséum, Paris et l'Académie des sciences, Paris  
*Comptes Rendus Palevol is a fast track journal published by the Museum Science Press, Paris and the Académie des sciences, Paris*

Les Publications scientifiques du Muséum publient aussi / *The Museum Science Press also publish:*

*Adansonia, Geodiversitas, Zoosystema, Anthropolozologica, European Journal of Taxonomy, Naturae, Cryptogamie* sous-sections *Algologie, Bryologie, Mycologie*.

L'Académie des sciences publie aussi / *The Académie des sciences also publishes:*

*Comptes Rendus Mathématique, Comptes Rendus Physique, Comptes Rendus Mécanique, Comptes Rendus Chimie, Comptes Rendus Géoscience, Comptes Rendus Biologies*.

Diffusion – Publications scientifiques Muséum national d'Histoire naturelle

CP 41 – 57 rue Cuvier F-75231 Paris cedex 05 (France)

Tél.: 33 (0)1 40 79 48 05 / Fax: 33 (0)1 40 79 38 40

[diff.pub@mnhn.fr](mailto:diff.pub@mnhn.fr) / <https://sciencepress.mnhn.fr>

Académie des sciences, Institut de France, 23 quai de Conti, 75006 Paris.

© Publications scientifiques du Muséum national d'Histoire naturelle / © Académie des sciences, Paris, 2021  
ISSN (imprimé / print): 1631-0683/ ISSN (électronique / electronic): 1777-571X

# New sperm whale remains from the late Miocene of the North Sea and a revised family attribution for the small crown physeteroid *Thalassocetus* Abel, 1905

**Apolline ALFSEN**

Centre de recherche en paléontologie - Paris - CR2P (CNRS, MNHN, Sorbonne Université),  
Département Origines et évolution, Muséum national d'Histoire naturelle,  
57 rue Cuvier, F-75231 Paris cedex 05 (France)

**Mark BOSSELAERS**

Institut royal des Sciences naturelles de Belgique, D.O. Terre et Histoire de la Vie,  
rue Vautier 29, 1000 Brussels (Belgium)  
and Koninklijk Zeeuwsch Genootschap der Wetenschappen,  
Kousteensedijk 7, 4331 Middelburg (The Netherlands)

**Olivier LAMBERT**

Institut royal des Sciences naturelles de Belgique, D.O. Terre et Histoire de la Vie,  
rue Vautier 29, 1000 Brussels (Belgium)  
[olivier.lambert@naturalsciences.be](mailto:olivier.lambert@naturalsciences.be) (corresponding author)

Submitted on 21 April 2020 | Accepted on 8 July 2020 | Published on 11 October 2021

---

[urn:lsid:zoobank.org:pub:89BE92BD-5D5F-49F9-8835-6622B5C9D5DE](https://zoobank.org/pub:89BE92BD-5D5F-49F9-8835-6622B5C9D5DE)

---

Alfsen A., Bosselaers M. & Lambert O. 2021. — New sperm whale remains from the late Miocene of the North Sea and a revised family attribution for the small crown physeteroid *Thalassocetus* Abel, 1905. *Comptes Rendus Palevol* 20 (39): 807-822. <https://doi.org/10.5852/cr-palevol2021v20a39>

## ABSTRACT

In spite of a continuously expanding physeteroid fossil record, our understanding of the origin and early radiation of the two modern sperm whale families Kogiidae Gill, 1871 (including the pygmy and dwarf sperm whales, *Kogia* spp.) and Physeteridae Gray, 1821 (including the great sperm whale, *Physeter* Linnaeus, 1758) remains limited, especially due to the poorly resolved phylogenetic relationships of a number of extinct species. Among those, based on fragmentary cranial material from the late early to middle Miocene of Antwerp (Belgium, North Sea basin), the small-sized *Thalassocetus antwerpiensis* Abel, 1905 has been recognized for some time as the earliest branching kogiid. The discovery of a new diminutive physeteroid cranium from the late Miocene (Tortonian) of Antwerp leads to the description and comparison of a close relative of *T. antwerpiensis*. Thanks to the relatively young ontogenetic stage of this new specimen, the highly modified plate-like bones making the floor of its supracranial basin could be individually removed, a fact that greatly helped deciphering their identity and geometry. Close morphological similarities with *T. antwerpiensis* allow for the reassessment of several facial structures in the latter; the most important reinterpretation is the one of a crest-like structure, previously identified as a sagittal facial crest, typical for kogiids, and here revised as the left

**KEY WORDS**

Cetacea,  
Physeteridae,  
Kogiidae,  
*Thalassocetus*,  
late Miocene,  
North Sea.

posterolateral wall of the supracranial basin, comprised of the left nasal (lost in kogiids for which the postnarial region is known) and the left maxilla. Implemented in a phylogenetic analysis, the new anatomical interpretations result in the new Belgian specimen and *T. antwerpiensis* being recovered as sister-groups in the family Physeteridae. Consequently, the geologically oldest kogiids are now dated from the Tortonian, further extending the ghost lineage separating these early late Miocene kogiid records from the estimated latest Oligocene to earliest Miocene divergence of kogiids and physeterids.

**RÉSUMÉ**

*De nouveaux restes de cachalot du Miocène supérieur de la mer du Nord et une attribution de famille révisée pour le petit physétéroïde apical Thalassocetus Abel, 1905.*

Notre compréhension de l'origine et de la première radiation évolutive des deux familles de cachalots actuels, à savoir les Kogiidae Gill, 1871 (incluant les cachalots pygmées et nains, *Kogia* spp.) et les Physeteridae Gray, 1821 (incluant le grand cachalot, *Physeter* Linnaeus, 1758), reste limitée du fait de la mauvaise résolution des relations phylogénétiques entre un certain nombre d'espèces éteintes, et ce malgré l'amélioration constante du registre fossile des physétéroïdés. Au sein de ce registre fossile, sur la base de matériel crânien fragmentaire provenant d'Anvers (Belgique, bassin de la mer du Nord) et daté de la fin du Miocène inférieur au Miocène moyen, l'espèce *Thalassocetus antwerpiensis* Abel, 1905 a été identifiée en tant que kogiidé le plus basal. La découverte récente du crâne d'un petit physétéroïde dans le Miocène supérieur (Tortonien) d'Anvers donne lieu ici à la description et à la comparaison d'un proche parent de *T. antwerpiensis*. Grâce au stade ontogénétique relativement précoce de ce nouveau spécimen, les plaques osseuses extrêmement modifiées qui forment le bassin supracrânien ont pu être individuellement retirées, ce qui a grandement aidé à leur identification et à la compréhension de leur géométrie. Les similarités morphologiques notées entre ce spécimen et *T. antwerpiensis* permettent de nouvelles interprétations de plusieurs structures de la face de ce dernier. La plus importante révision concerne la structure en forme de crête identifiée précédemment comme la crête sagittale faciale, caractéristique des kogiidés; cette structure est ici identifiée comme le bord postérolatéral gauche du bassin supracrânien, constitué du nasal gauche (perdu chez les kogiidés chez lesquels la région post-nariale est connue) et du maxillaire gauche. Intégrées dans une analyse phylogénétique, ces interprétations anatomiques du nouveau spécimen belge et de *T. antwerpiensis* révèlent pour ceux-ci une relation de groupes frères dans la famille des Physeteridae. Par conséquent, les plus anciens kogiidés fossiles connus sont maintenant datés du Tortonien, ce qui allonge d'autant plus la lignée fantôme séparant les premières occurrences de kogiidés fossiles (début du Miocène supérieur) de la divergence entre kogiidés et physétéridés, estimée entre l'Oligocène terminal et le tout début du Miocène.

**MOTS CLÉS**

Cetacea,  
Physeteridae,  
Kogiidae,  
*Thalassocetus*,  
Miocène supérieur,  
mer du Nord.

**INTRODUCTION**

The two extant sperm whale genera, *Kogia* Gray, 1846 (dwarf and pygmy sperm whales) and *Physeter* Linnaeus, 1758 (sperm whale), are highly disparate, both in terms of their body size (standard length of 2.7 and 3.4 m in the two species of *Kogia*, whereas adult males of *Physeter macrocephalus* can reach a length of 18 m) and in terms of head morphology (Rice 1989; Heyning 1989; Caldwell & Caldwell 1989; Cranford *et al.* 1996; Huggenberger *et al.* 2016). These marked differences lead to the placement of these two genera in separate families, Kogiidae Gill, 1871 and Physeteridae Gray, 1821, within the superfamily Physeteroidea (e.g. Muizon 1991; Bianucci & Landini 2006). However, it is expected that when returning to the earliest steps of their evolutionary history, basal kogiids and physeterids would prove much less easy to distinguish. Originating from Miocene deposits of the Antwerp area (Belgium, southern margin of the North Sea basin), the fragmentarily known *Thalassocetus antwerpiensis*

Abel, 1905 was first identified as a non-kogiid sperm whale (Abel 1905; Kazár 2002; see also some elements of comparison with *Orycterocetus* Leidy, 1853 in Kellogg 1965). It was later tentatively referred to the family Kogiidae, due to its small size and the description of a sagittal facial crest in the supracranial basin of the lectotype specimen (Bianucci & Landini 2006; Lambert 2008). This referral was confirmed in later phylogenetic analyses (e.g. Velez-Juarbe *et al.* 2015; Collareta *et al.* 2017a; Lambert *et al.* 2017; Benites-Palomino *et al.* 2020; Paolucci *et al.* 2020), making *Thalassocetus* one of the most basal kogiids, and possibly the geologically oldest kogiid, which made it an important taxon (though a fragmentarily known one) for the early evolution of this clade. In the present work we describe a small physeteroid cranium recently discovered in late Miocene deposits of the Antwerp suburbs. Its comparison with the *Thalassocetus* Abel, 1905 type material leads to a new interpretation of the facial morphology of the latter, allowing for a reappraisal of its systematic position and phylogenetic relationships.

## MATERIAL AND METHODS

## STUDIED MATERIAL

Discovered in non-indurated sand, the studied skull IRSNB M.2329 was easily freed from the surrounding sediment with a soft brush. Preserved as many small fragments, it has been reassembled by M.B. in two main parts, the facial region and the right side of the basicranium. Three thin, plate-like elements making the floor of the supracranial basin were kept free from the main facial part, allowing for the observation of underlying bones (see description below).

## INSTITUTIONAL ABBREVIATIONS

IRSNB Institut royal des Sciences naturelles de Belgique, Brussels;  
MUSM Museo de Historia Natural, Universidad Nacional Mayor de San Marco, Lima.

## PHYLOGENETIC ANALYSIS

To test the phylogenetic relationships of the new specimen, we coded it in the character/taxon matrix of Collareta *et al.* (2019) including 53 morphological characters (Appendices 1; 2). The resulting number of ingroup physeteroid taxa is 26, in addition to three outgroups, namely, the basilosaurids *Cynthiacetus* Uhen, 2005 and *Zygorhiza* True, 1908, and the archaic odontocete *Agorophius* Cope, 1895. Based on our new interpretation of the lectotype's cranial morphology, we corrected seven codings for *Thalassocetus antwerpiensis* (characters 3, 13, 14, 19, 21, 26 and 30). Our heuristic search was performed with Paup 4.0 (Swofford 2001), following the method of Collareta *et al.* (2019) with all characters unordered and equally weighted, and all default settings (including TBR with reconnection limit = 8 and ACCTRAN optimization). Node support was evaluated through calculation of bootstrap values (100 replicates).

## SYSTEMATIC PALAEOLOGY

Order CETACEA Brisson, 1762  
Clade PELAGICETI Uhen, 2008  
Clade NEOCETI Fordyce & Muizon, 2001  
Suborder ODONTOCETI Flower, 1867a  
Superfamily PHYSETEROIDEA Gray, 1821  
Family PHYSETERIDAE Gray, 1821

*Thalassocetus* Abel, 1905

*Thalassocetus* Abel, 1905: 70.

TYPE SPECIES. — *Thalassocetus antwerpiensis* Abel, 1905.

DIAGNOSIS. — Same as for the sole currently described species *T. antwerpiensis*.

*Thalassocetus antwerpiensis* Abel, 1905

*Thalassocetus antwerpiensis* Abel, 1905: 70.

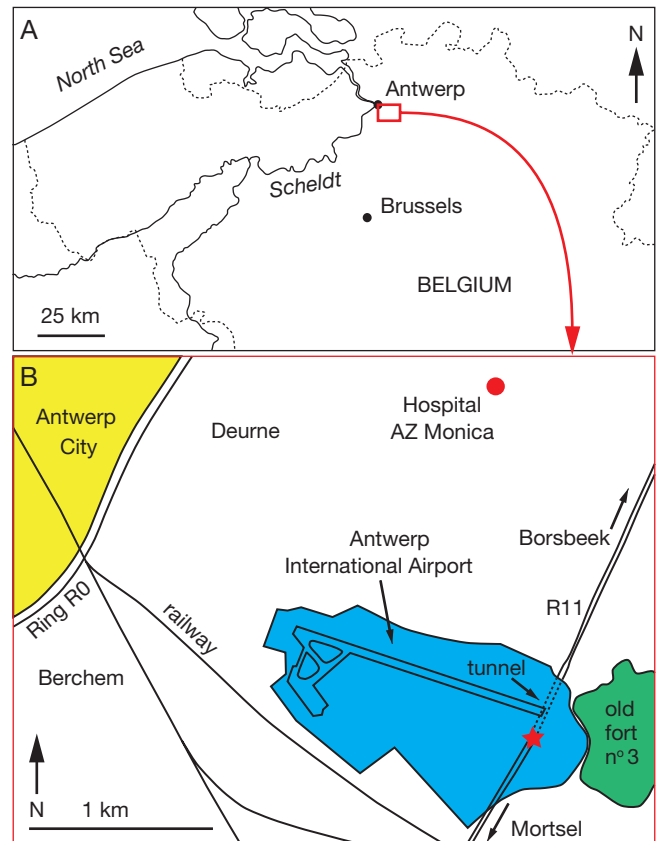


FIG. 1. — **A**, Schematic geographic map of the North of Belgium showing the position of Antwerp, the area where the lectotype of *Thalassocetus antwerpiensis* Abel, 1905 IRSNB M.525 was discovered (no precise locality recorded); **B**, detail map of the southeastern suburbs of Antwerp, indicating the locality (red star) where *Thalassocetus* sp. IRSNB M.2329 was found, during the excavation of a tunnel on the road R11 between Mortsel and Borsbeek, along the Antwerp International Airport. The fossil site of the hospital AZ Monica (Deurne), where a glauconitic sand layer similar to the one having yielded IRSNB M.2329 was observed, is marked by a red point.

LECTOTYPE. — IRSNB M.525, a fragmentary cranium including part of the supracranial basin, the right orbit, and the right part of the basicranium.

TYPE HORIZON AND AGE. — An origin in the Berchem Formation, possibly the Antwerpen Sands Member, dated from the late early to middle Miocene (late Burdigalian to Langhian; Louwye 2005; Louwye *et al.* 2010), has been tentatively proposed by Lambert (2008), based on color and preservation state.

TYPE LOCALITY. — Antwerp area (Fig. 1). No precise locality recorded.

EMENDED DIAGNOSIS. — This small size physeterid (postorbital width lower than 300 mm in the juvenile to subadult lectotype, within the range of adults of *Kogia* spp.) can be distinguished from all other physeteroids (stem physeteroids, physeterids, and kogiids) by the following unique combination of cranial morphological features: antorbital notch being located outside the proportionally narrow supracranial basin (differing from most kogiids); at least one right dorsal infraorbital foramen being located inside the supracranial basin; retention of the left nasal along the left posterolateral wall of the supracranial basin (differing from kogiids for which the postnasal region is known); left nasal being posteriorly pointed, with the apex nearly reaching the nuchal crest and being close to the sagittal plane of the cranium (differing, among others, from *Orycterocetus crocodilinus* Cope, 1868); absence of a sagittal facial crest in the supracranial

basin (differing from most kogiids); abrupt dorsal elevation of the posterior part of the maxilla towards the nuchal crest; short, triangular zygomatic process of the squamosal (ratio between distance from anterior tip of zygomatic process to exoccipital and postorbital width lower than 0.25); nodular, somewhat anteroposteriorly thickened postglenoid process of the squamosal; anteroposteriorly short posttympanic process of the squamosal, lacking a broad notch for the posterior process of the tympanic (differing from most kogiids); and anterodorsal portion of the surface of the occipital shield being dorsoventrally concave and transversely convex.

*Thalassocetus* sp.

REFERRED SPECIMEN. — IRSNB M.2329, a fragmentary cranium including the rostrum base, most of the facial region, and the right part of the basicranium.

HORIZON AND AGE. — IRSNB M.2329 originates from a yet unnamed lithological unit (layer V of Hoedemakers & Dufrain 2015; but see Goolaerts *et al.* 2020 for further details) made of fine, blue-grey glauconitic sand, that is currently interpreted as being intercalated between the upper layers of the Antwerpen Sands Member (Berchem Formation) and the base of the Deurne Sands Member (Diest Formation). No biostratigraphic analysis of this unit has been published yet, but the upper age limit of the Antwerpen Sands and the lower age limit of the Diest Formation may constrain it to an interval ranging from about 11.3 to 9 Ma (early Tortonian, earliest late Miocene; Louwye 2005; Louwye *et al.* 2007). It is for now not possible to completely exclude the possibility that this unit corresponds to an unknown lower part of the Diest Formation (as later confirmed in Goolaerts *et al.* 2020; in this case its upper age limit may fall in the interval ranging from 9 to 7.5 Ma (late Tortonian; Louwye *et al.* 2007). This unit matches well the sedimentological and palaeontological features of a coarse grey-green glauconitic sand level temporarily exposed during construction work at the hospital AZ Monica, campus Deurne, located 2.3 km north to the R11 tunnel site (Bosselaers *et al.* 2004; level f; M.B., pers. obs.; Fig. 1). Tentatively interpreted in that earlier work as corresponding to a lower portion of the Deurne Sands Member, this level yielded fossil cetacean remains including the articulated skeleton of a large cetotheriid (identified as *Plesiocetus* sp. in Bosselaers *et al.* 2004) and the cranium of a ziphiid (identified as *Ziphirostrum marginatum* in Lambert 2005).

LOCALITY. — IRSNB M.2329 was discovered in 2014 by Leo Dufrain during excavations for a tunnel on the road R11 between Mortsel and Borsbeek, along the Antwerp International airport (Fig. 1). Geographic coordinates: 51°11'08"N, 4°28'18"E.

COMMENTS

This specimen shares all the diagnostic features of *Thalassocetus antwerpiensis* as listed above. However, because of: 1) a series of minor morphological differences (see below; width of right maxilla between antorbital notch and largest dorsal infraorbital foramen, aspect of anterodorsal surface of left nasal, shape of lateral surface of postorbital process of frontal, and degree of concavity of posterior surface of exoccipital); 2) the fragmentary state of the lectotype of *Thalassocetus antwerpiensis*; and 3) a possibly older geological age for the latter, we choose to provisionally keep an open taxonomic attribution for IRSNB M.2329. It may either belong to the species *T. antwerpiensis*, or to a new, closely related taxon. The second option would mean that the diagnosis proposed above would apply to the genus *Thalassocetus*, whereas a new diagnosis would have to be proposed for each species in that genus.

DESCRIPTION OF *THALASSOCETUS* SP. IRSNB M.2329

*General morphology and ontogenetic stage*

From the supraoccipital to the anterior edge of the truncated vomer the cranium has a preserved length of 314 mm and a postorbital width of 281 mm. The small size of the cranium and the unfused sutures between all the bones suggest that this specimen was a juvenile. It is relatively small for a physeteroid, close to cranial dimensions of extant dwarf and pygmy sperm whales (*Kogia* spp.), in which adults can reach a cranium width of 245 mm for *Kogia sima* (Owen, 1868) and 378 mm for *Kogia breviceps* (Blainville, 1838) (Ross 1984). However, based on the preserved parts we can assume that the rostrum length of this specimen was greater than in *Kogia* spp. Also, the supracranial basin is markedly smaller than in the latter: the crests that laterally delimit the basin have a more medial position, not reaching the antorbital region and not including the right and left antorbital notches inside the basin (Fig. 2), as opposed to *Kogia* spp. (e.g. Velez-Juarbe *et al.* 2015). The supracranial basin is delimited on the right side by the right maxilla, on the posterior side by the right premaxilla, and on the left side by the left maxilla (posteriorly) and left premaxilla (anteriorly). With a maximum width of 141 mm between the right and left margins (approximately equivalent to half the postorbital width), the basin is about as wide as long, not extending anteriorly beyond the right premaxillary foramen, its anterior boundary being rather defined by a dorsomedial elevation of the right premaxilla and vomer (see below). The floor of the supracranial basin is mainly made by the right premaxilla. Between the highly asymmetrical bony nares (the left naris being much larger than the right one), the presphenoid closes posteriorly the broad mesorostral groove. In the reconstructed lateral view (Fig. 3), the temporal fossa appears as slightly higher than anteroposteriorly long, in a way similar to *Orycterocetus*.

*Premaxilla*

The strong asymmetry of this cranium is especially expressed in the organization of the premaxillae in the supracranial basin. Only the posterior part of the left premaxilla is preserved, displaying strong similarities with *Orycterocetus crocodilinus* (Kellogg 1965). The premaxilla forms the anterior part of the left lateral wall of the supracranial basin, where it wedges into a groove of the maxilla as in *Orycterocetus*. On the other hand, the right premaxilla has a much larger posterior extent, as a roughly transversely flat and anteroposteriorly concave broad plate that reaches the posterodorsal margin of the supracranial basin and the base of both the lateral walls of the basin, in a way similar to *Orycterocetus*. The surface of the supracranial basin is therefore smooth, lacking any indication of a sagittal facial crest, a feature described in all kogiids (Velez-Juarbe *et al.* 2015; Collareta *et al.* 2017a). In lateral view, from the anterior edge of the right bony naris to the posterodorsal edge of the basin, the right premaxilla raises posterodorsally with an approximate angle of 110° with respect to the long axis of the rostrum.

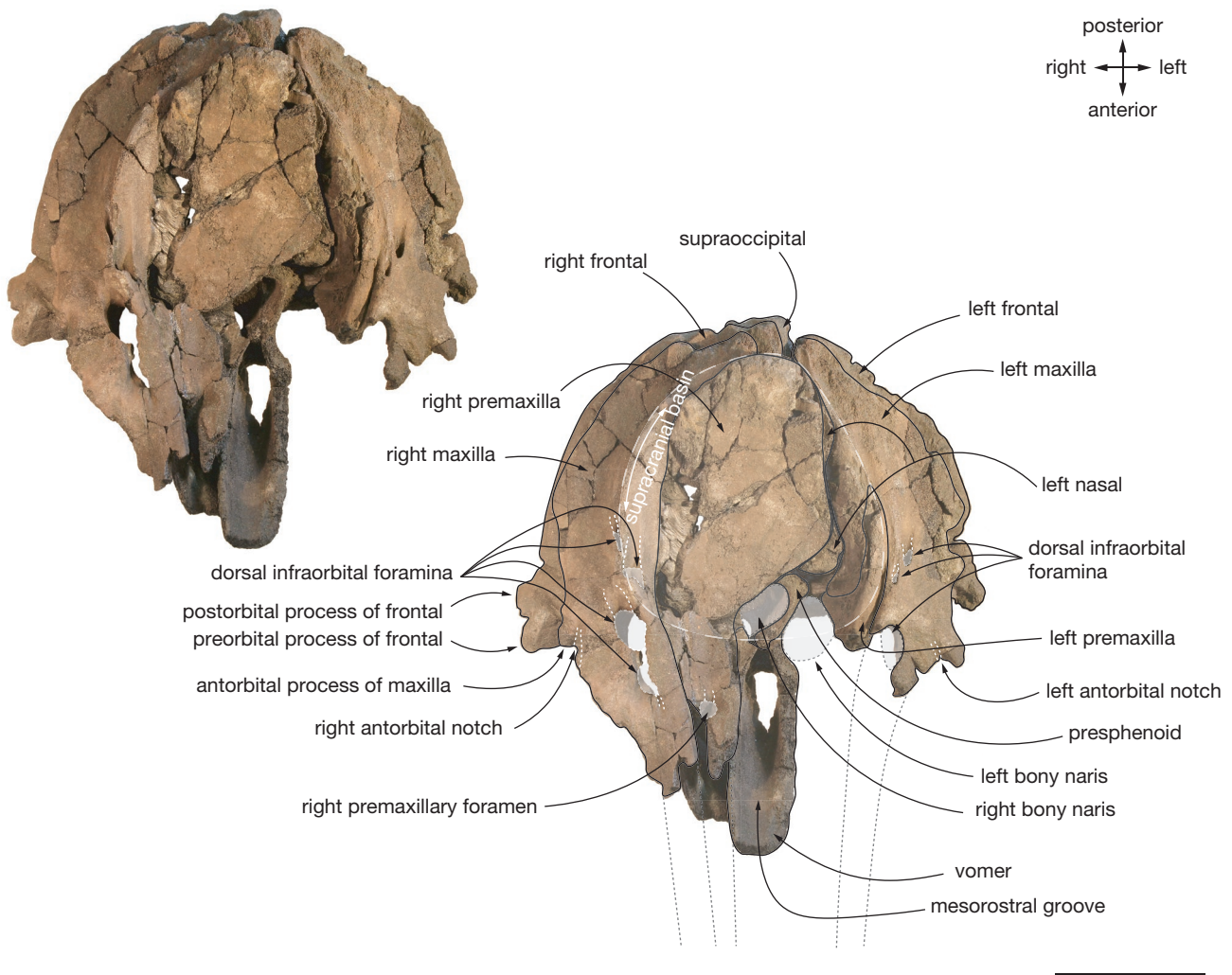


FIG. 2. — Cranium of *Thalassocetus* sp. IRSNB M.2329 (early late Miocene, Antwerp suburbs, Belgium) in anterodorsal view. **Black dotted lines** for the reconstructed outline of the rostrum and some foramina; **white dotted lines** for sulci; **grey dotted lines** for the outline of the supracranial basin. Scale bar: 100 mm.

Only the right premaxilla is preserved anterior to the antorbital notch. Transversely narrower than the right maxilla, it is pierced by a large premaxillary foramen that is located about 30 mm anterior to the level of the antorbital notch, anterior to the anteriormost right dorsal infraorbital foramen (as in *Orycterocetus*).

#### Maxilla

Lateral to the crests defining the supracranial basin, both maxillae become gradually dorsoventrally thinner towards the lateral edges of the cranium. They are asymmetrical at this level: this lateral part is slightly wider on the left maxilla (62 mm vs 56.5 mm on the right side, posterior to the posteriormost dorsal infraorbital foramina) and the dorsal surface is more transversely concave on the right side. The right and left maxillae almost contact each other along the posterior wall of the supracranial basin, behind the right premaxilla. The right maxilla displays four dorsal infraorbital foramina. The small, posteriormost of these foramina is located just

lateral to the maxillary crest defining the supracranial basin and it is followed posteriorly by a long groove along the basin's margin. The second foramen is larger and located on the wall of the basin, just posterior to the level of the corresponding antorbital notch. Placed at the level of the antorbital notch, the third foramen is the largest. The narrower fourth foramen is located anterior to the notch and preceded anteriorly by two grooves at the rostrum base. The preserved portion of the left maxilla exhibits three dorsal infraorbital foramina, all located outside the supracranial basin. The posteriormost of these foramina is also followed posteriorly by a groove, which is shorter than that on the right side. Just anteromedial, the second foramen is markedly smaller, whereas the third is only partly preserved, but was originally the largest, located at the level of the antorbital notch. Lateral to the right dorsal infraorbital foramina a series of small depressions/fossae likely indicate insertions of facial muscles (red dotted lines in Figure 3). The short, broadly open antorbital notch is followed posteriorly by a short sulcus; it differs markedly

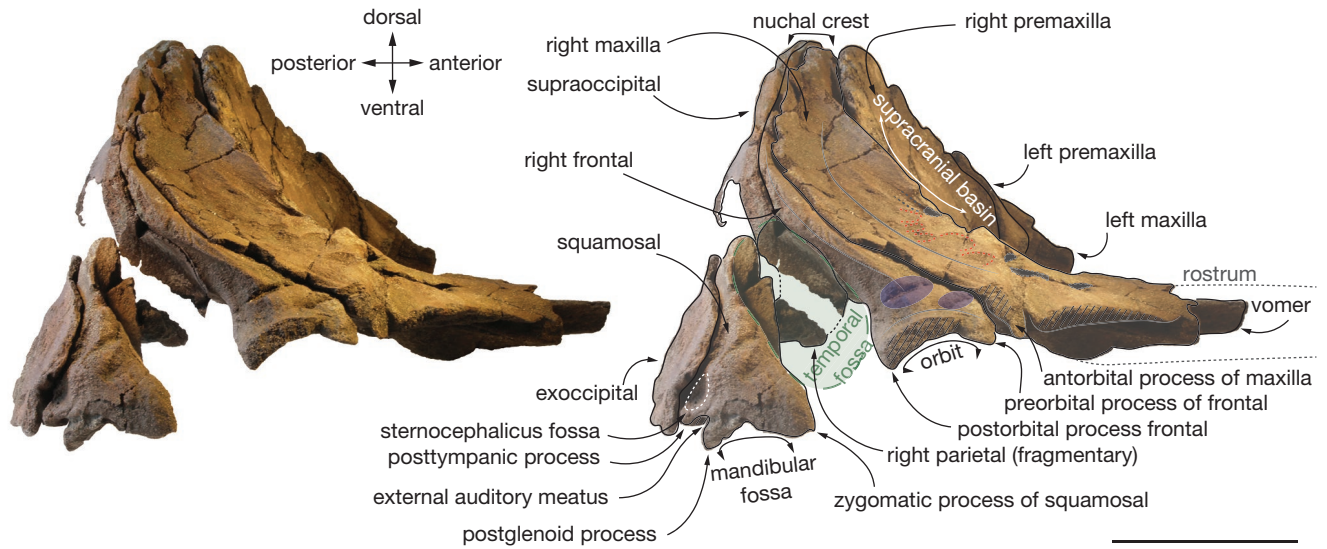


FIG. 3. — Cranium of *Thalassocetus* sp. IRSNB M.2329 (early late Miocene, Antwerp suburbs, Belgium) in right lateral view. Hatching for break surfaces; **grey dotted lines** for the reconstructed outline of the rostrum; **green dotted line** for the outline of the temporal fossa; **mauve shaded areas** for shark bite marks; **red dotted lines** for areas of origin of facial muscles. Scale bar: 100 mm.

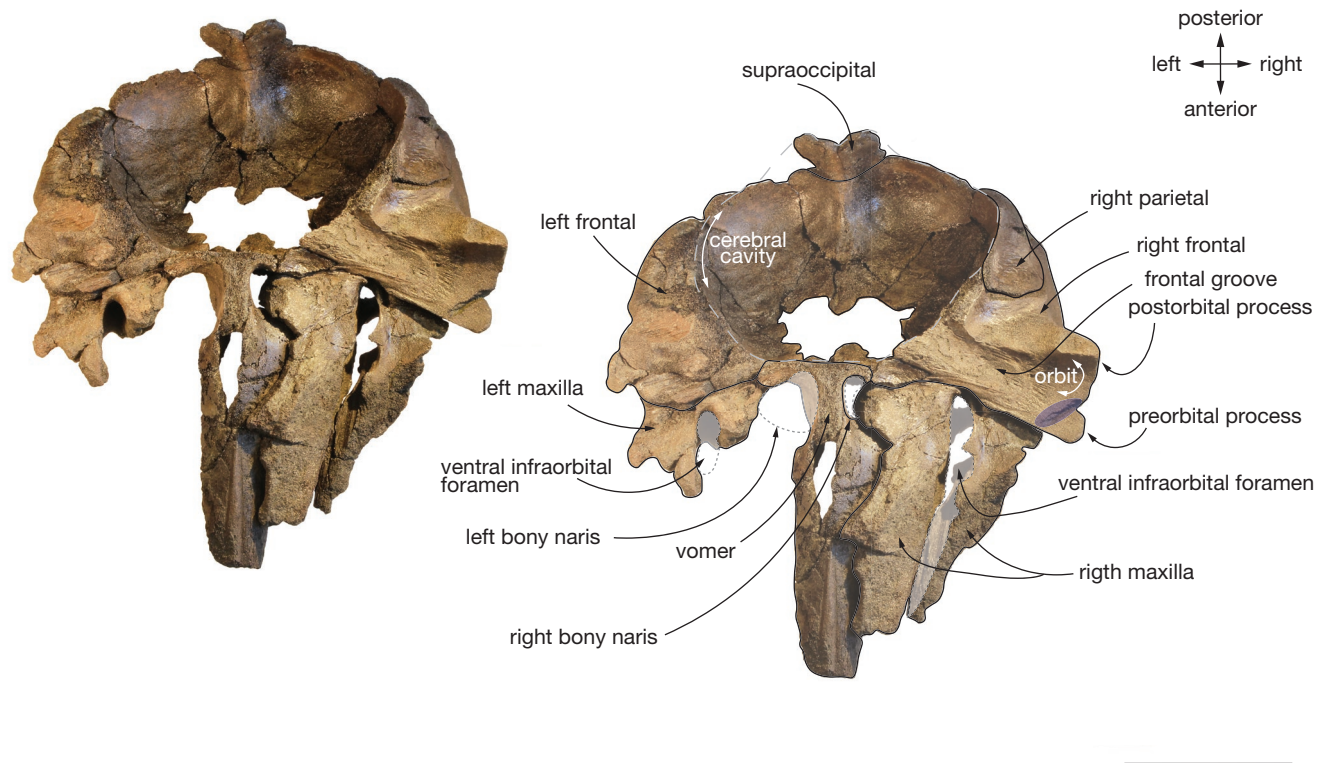


FIG. 4. — Cranium of *Thalassocetus* sp. IRSNB M.2329 (early late Miocene, Antwerp suburbs, Belgium) in ventral view. **Grey dotted lines** for foramina and for the outline of the cerebral cavity; **mauve shaded areas** for bite marks. Scale bar: 100 mm.

from the “slit-like” notch of *Kogia* and several extinct kogiids (*Koristocetus* Collareta, Lambert, Muizon, Urbina & Bianucci, 2017, *Nanokogia* Velez-Juarbe, Wood, Gracia & Hendy, 2015, *Pliokogia* Collareta, Cigala Fulgosi & Bianucci, 2019,

and Scaphokogiinae Muizon, 1988), and it is more similar to the notch seen, for example, in *Orycterocetus* and *Physeter*. In lateral view, the maxillae get gradually thinner along their oblique posterodorsal ascent from the antorbital notch

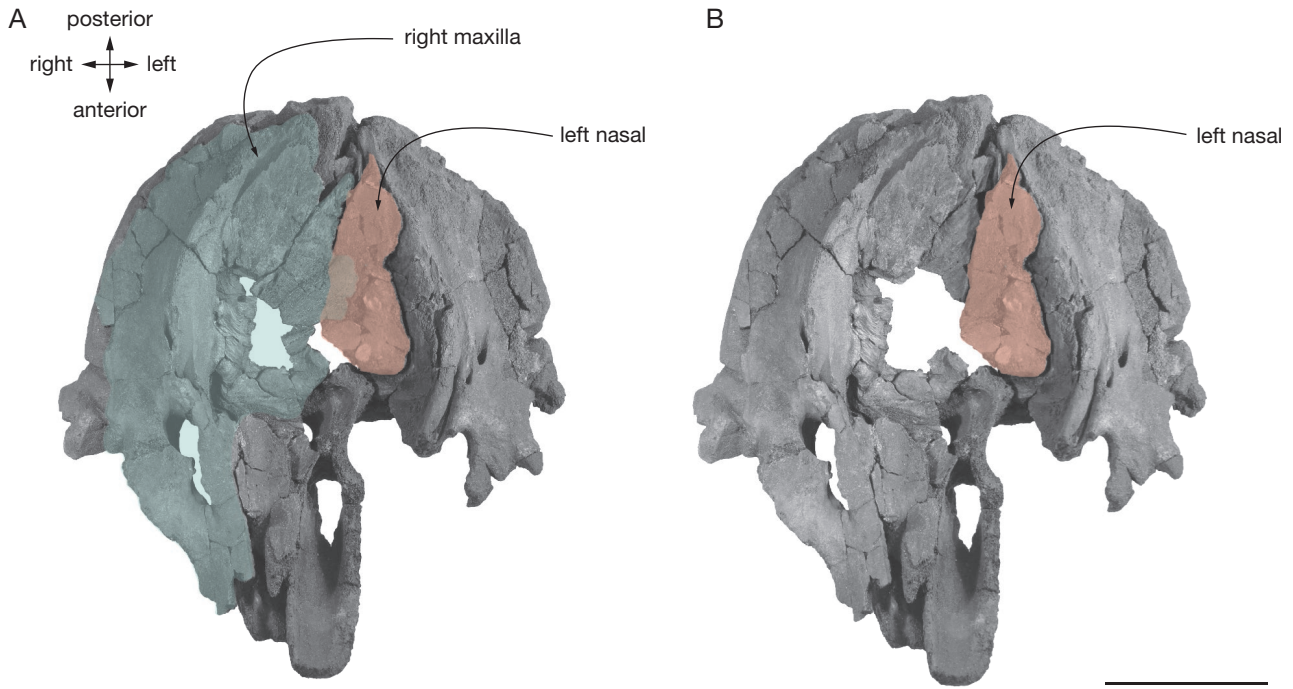


FIG. 5. — **A**, Cranium of *Thalassocetus* sp. IRSNB M.2329 (early late Miocene, Antwerp suburbs, Belgium) in anterodorsal view with part of the right premaxilla removed and right maxilla highlighted in **green**; **B**, same view with part of the right maxilla removed; left nasal is highlighted in **red**. Scale bar: 100 mm.

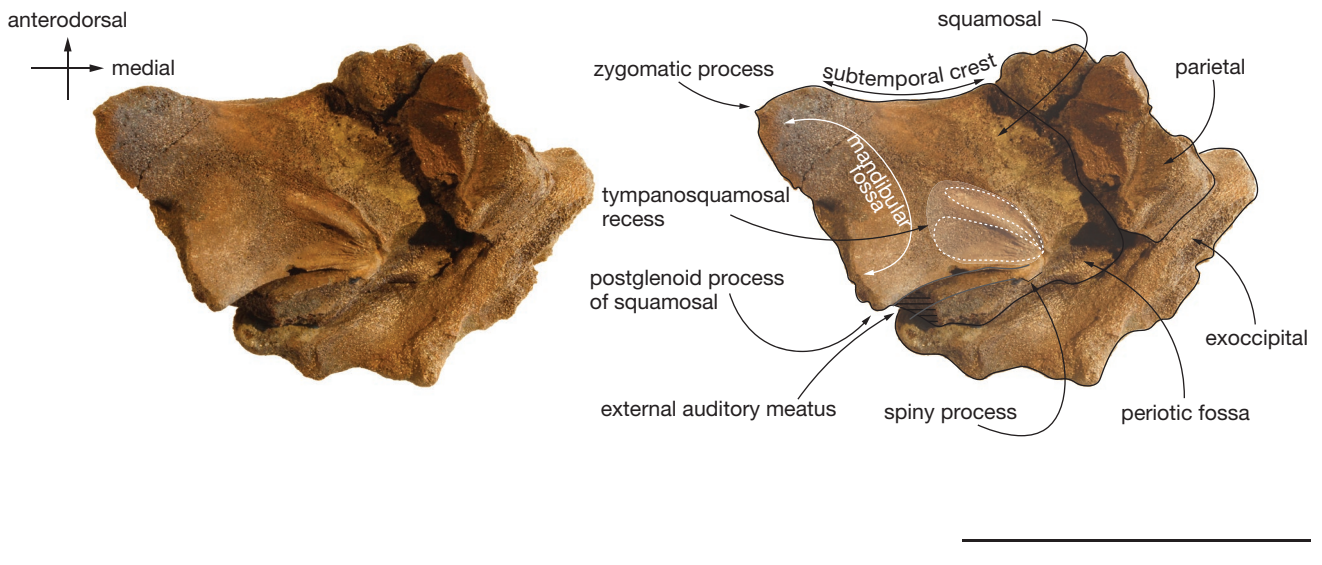


FIG. 6. — Right squamosal of *Thalassocetus* sp. IRSNB M.2329 (early late Miocene, Antwerp suburbs, Belgium) in ventromedial view. **White dotted lines** for deeper areas of the tympanosquamosal recess; hatching for break surfaces. Scale bar: 100 mm.

to the nuchal crest, where their long axis almost reaches a vertical orientation.

In ventral view, the maxillae are only partly preserved along the rostrum base, where they cover the vomer ventrally (Fig. 4). Anteriorly, the maxillae are too damaged for the presence of an alveolar groove and of alveoli for functional teeth to be assessed. Other bones of the palate (palatines and pterygoids) are not preserved.

*Vomer*

At the rostrum base, the thick vomer makes the ventral and lateral walls of a broad, U-shaped mesorostral groove. In dorsal view the raised medial edge of the right premaxilla covers the lateral wall of the groove. Bones that originally covered the vomer ventrally are missing but a medial crest is present on the latter, suggesting that this ventralmost part of the vomer was exposed ventrally between the right and the left maxillae (as often occurs in odontocetes).

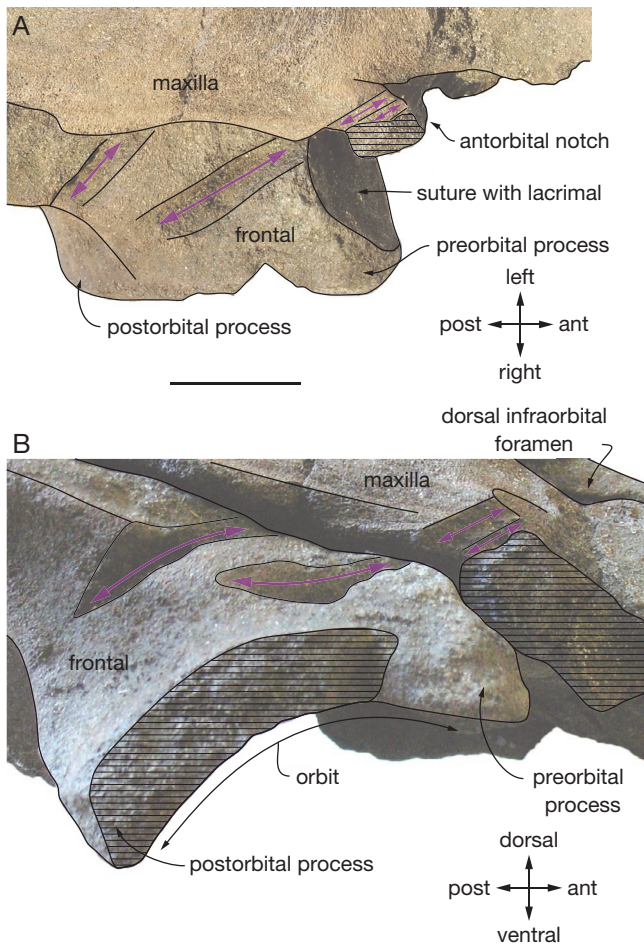


FIG. 7. — Detail views of the right orbit region of *Thalassocetus* sp. IRSNB M.2329 (early late Miocene, Antwerp suburbs, Belgium) in dorsal (A) and right lateral view (B), showing the deep grooves interpreted as shark bite marks (mauve arrows). Hatching for break surfaces. Scale bar: 20 mm.

### Frontal

In dorsal view, frontal bones are only visible at the lateral edge of the neurocranium, in the supraorbital area and anterior to the nuchal crest. At the level of the nuchal crest the right and left frontals contact each other along the sagittal plane.

Only the right frontal has the preorbital and postorbital processes preserved. Moderately thickened dorsoventrally, the short preorbital process is separated from the partly preserved antorbital process of the maxilla by a narrow notch, at least 12 mm deep. The latter was originally occupied by the lacrimal, which is missing on this specimen.

Somewhat laterally and ventrally truncated, the postorbital process is directed ventrally. Posterior to this process the frontal gets dorsoventrally thinner while raising posterodorsally above the temporal fossa. In lateral view of the supraorbital region the maxilla-frontal suture draws an angle of about 30° with the horizontal plane of the rostrum. In the posterodorsal quarter of the frontal, where the latter is sandwiched between maxilla and supraoccipital, this suture reaches an almost vertical orientation.

In ventral view, the frontals outline the cerebral cavity anterodorsally. This cavity has a cordiform shape, with a maximum

width of 177 mm and a length of 124 mm. Ventral to the right frontal a part of the parietal bone is preserved (Fig. 4).

### Nasal

This specimen has two bony nares but only one nasal (the left one), as reported for part, but not all non-kogiid physeteroids (two nasals are recorded in part of the stem physeteroids and no nasal is observed in kogiids; Flower 1867b; Kellogg 1965; Velez-Juarbe *et al.* 2015; Lambert *et al.* 2017; Collareta *et al.* 2017a). This nasal being fully accessible thanks to the unfused, removable plate-like posterior part of the right premaxilla and posteromedial part of the right maxilla in the supracranial basin (Fig. 5), we could clearly see that this bone is located between the sagittal plane and the left margin of the supracranial basin, posterior to the left bony naris and the presphenoid. Extending to the posterior edge of the basin, this dorsoventrally thin bone thickens slightly medially and, to a greater extent, anterolaterally towards the posterior margin of the left bony naris. The nasal is 118 mm long and 54 mm wide; it contributes to approximately 77% of the length of the supracranial basin. In dorsal view, with the overlying right maxilla and premaxilla in place, the nasal is only visible in its anterolateral and posterolateral regions, which poke out under the right premaxilla. The thin left edge of the nasal covers the left maxilla along the lateral wall of the supracranial basin, while its right edge is sutured in its anterior half with the right frontal and in its posterior half with the right maxilla. Ventrally the nasal bone mainly rests on the left frontal.

### Supraoccipital

With a partly abraded outer surface, the supraoccipital is mostly preserved on the upper part of the occipital shield. This region is dorsoventrally concave and slightly transversely convex, drawing an angle of approximately 70° with respect to the long axis of the rostrum in lateral view. Along with the frontals and maxillae the upper edge of the supraoccipital constitutes a thick nuchal crest whose dorsomedial portion projects posterodorsally.

### Squamosal

Only a part of the right side of the basicranium is preserved, detached from the rest of the cranium. Its position and orientation relative to the main dorsal fragment has been interpreted based on the orientation of the surfaces of the squamosal and parietal on both sides of the fracture zone (Fig. 3). It is mostly comprised of the squamosal and exoccipital, with a small fragment of parietal preserved in the posterodorsolateral corner of the cerebral cavity. In lateral view the zygomatic process has a triangular shape and its apex is anteriorly directed. The zygomatic process is proportionally short, with a distance from the anterior tip to the squamosal exoccipital suture of 66 mm. The supramastoid crest gradually raises posterodorsally towards the temporal crest, as in many other physeteroids (Bianucci & Landini 2006). Medially, the narrow squamosal fossa is anteroposteriorly and transversely concave. The short and slender postglenoid process is an anteroposteriorly thin

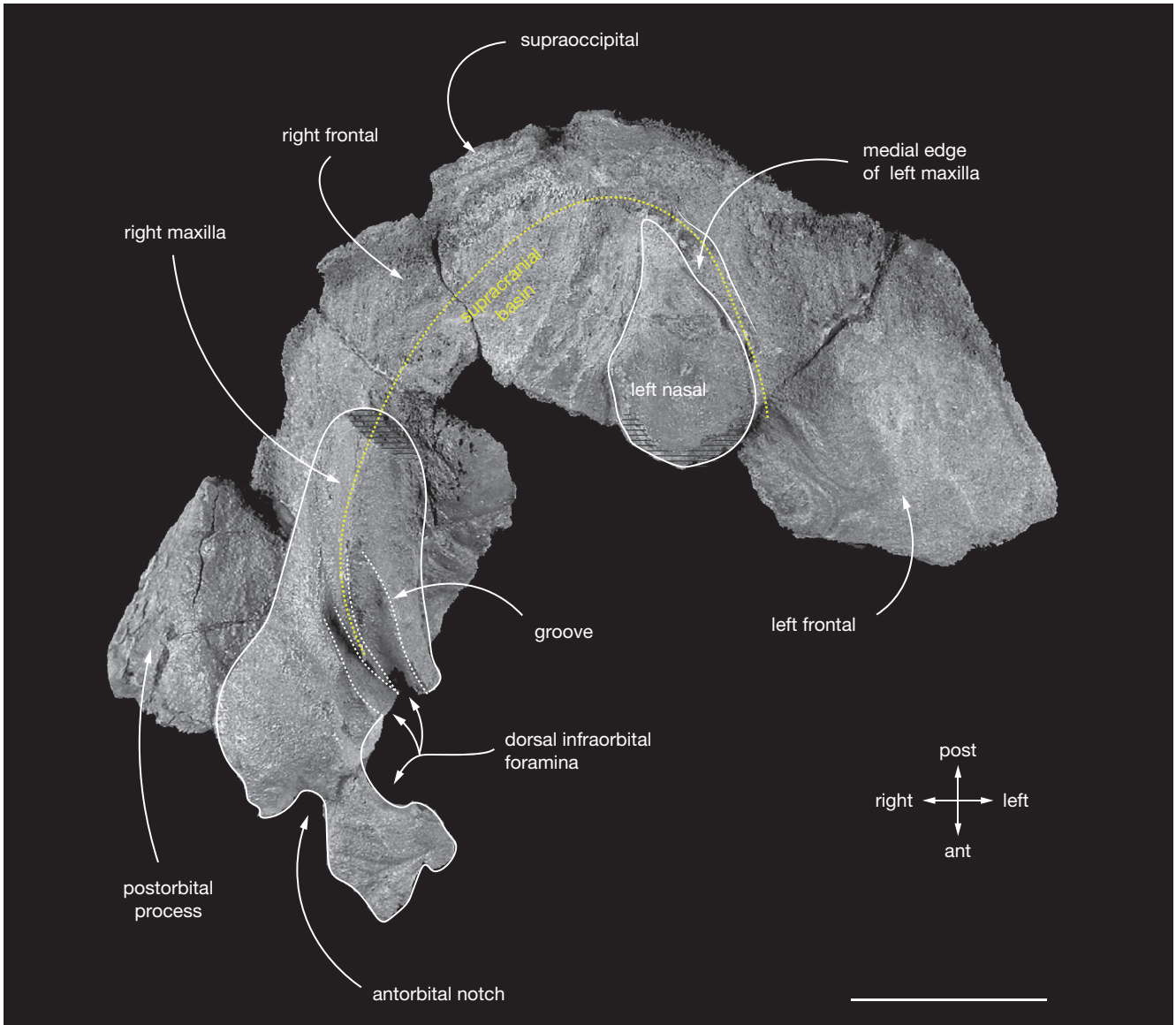


FIG. 8. — Revised interpretation of the osteoanatomical features of the cranium of *Thalassocetus antwerpiensis* Abel, 1905 IRSNB M.525 (lectotype, late early to middle Miocene, Antwerp area, Belgium) in anterodorsal view. Hatching for break surfaces; **yellow dotted line** for the outline of the supracranial basin; **white dotted lines** for sulci. Scale bar: 50 mm.

plate that anteriorly defines a deep and narrow external auditory meatus. Between this meatus and the anteroventral margin of the exoccipital, the posttympanic process is short (maximum anteroposterior length in ventral view equals 15 mm), leaving a space for the posterior process of the tympanic ventral to the posttympanic process that is much more limited than in *Kogia* spp. and related taxa (e.g. Velez-Juarbe *et al.* 2015). The posttympanic process was reaching approximately the same dorsoventral level as the postglenoid process. In ventral view, the mandibular fossa is moderately concave dorsoventrally and poorly separated from the tympanosquamosal recess (Fig. 6). The latter displays two oblique, anterolaterally elongated fossae separated by a thick and low crest. The deepest and broadest fossa is the posterolateral one, located along the anterior meatal crest. Most of the falciform process of the squamosal and the alisphenoid are missing.

#### Exoccipital

In lateral view the ventralmost region of the preserved basi-cranium is made by the exoccipital. The preserved part of this bone is lateral to the missing right occipital condyle. Posteriorly and slightly laterally, it covers the squamosal as an anteroposteriorly thin plate with a roughly flat, slightly anteriorly tilted posterior surface. In ventral view the paroccipital process is weakly thickened.

#### Potential bite marks

Two deep and broad, subparallel oblique grooves running posterolaterally on the dorsal surface of the right frontal above the orbit (Figs 3; 7) may correspond to healed bite marks, possibly by a large shark (for examples of shark bites on fossil marine mammal bones, see Bianucci *et al.* 2010; Collareta *et al.* 2017b; for putative healing of a bite on cetacean bone, see Kallal *et al.*

2012). The flanks of these grooves with a V-shaped section are indeed made of compact bone with a smooth surface, contrasting with other, postmortem damage in the frontal, revealing more spongy bone, and suggesting therefore that some post-bite bone repair may have occurred. The anterior groove extends on a short distance on the lateral edge of the maxilla, where it appears as two narrower, parallel grooves (Fig. 7). Ventrally, the preorbital region of the right frontal is also deeply cut by a groove that is similarly directed posterolaterally (Fig. 4); this groove is thus interpreted as resulting from the same biting event (opposite tooth).

#### COMPARISON WITH *THALASSOCETUS*

Originating from the same geographic region (southern North Sea Basin) as the lectotype of *Thalassocetus antwerpiensis* IRSNB M.525, and possibly from a slightly younger horizon, IRSNB M.2329 shares with the latter a series of morphological features. First of all, their size is very similar (postorbital width estimated to 280–290 mm and 280 mm for *T. antwerpiensis* and IRSNB M.2329, respectively; Lambert 2008; this work). In addition, based on the degree of fusion of the cranial sutures (e.g. frontals, maxillae, and premaxillae not fused) they most likely do not correspond to markedly different ontogenetic stages. More specifically, the right lateral side of the small supracranial basin, comprised of the right maxilla, is nearly identical in terms of: 1) the extent of the lateral crest on the maxilla; 2) the size and position of the dorsal infraorbital foramina and their associated grooves; and 3) the shape of the antorbital notch (Fig. 8). In contrast with the interpretation proposed by Lambert (2008: fig. 16, but see fig. 18), the right maxilla of the lectotype of *T. antwerpiensis* is posteriorly incomplete, but the surface of the underlying frontal indicates a strong elevation of the posteriormost part of the maxilla towards the nuchal crest that is highly similar to the condition observed in IRSNB M.2329. The short zygomatic process of the squamosal, the supramastoid crest, and the squamosal fossa are also nearly identical in these two specimens, and the same can be said for the frontals and supraoccipital along the nuchal crest. All these strong anatomical similarities point to close relationships between IRSNB M.525 and IRSNB M.2329 (see also the phylogenetic analysis below) and allow for a reinterpretation of the bones preserved in the supracranial basin of the lectotype of *T. antwerpiensis*.

The feature that has been interpreted as a sagittal crest in the lectotype of *T. antwerpiensis* (Bianucci & Landini 2006; Lambert 2008) corresponds very well to the left posterolateral edge of the supracranial basin of IRSNB M.2329. It actually appears somewhat more prominent in the lectotype of *T. antwerpiensis* due to the loss of most of the left maxilla outside of the basin. With such a reinterpretation of the sagittal crest as a whole, different sub-parts can be discussed. The region that was identified as a shallow fossa in the right premaxilla of the lectotype of *T. antwerpiensis* (corresponding to the premaxillary fossa of Barnes 1973) is actually very similar in outline and position to the triangular posterodorsal end of the left nasal of IRSNB M.2329, whereas the upturned median plate of the left maxilla in the lectotype of *T. antwerpiensis* matches

the orientation of the crest on the left maxilla defining the posterolateral margin of the supracranial basin. Medial to the bone reinterpreted here as the left nasal, the dorsal surface of the right frontal of the lectotype of *T. antwerpiensis* displays suture marks for the attachment of the right maxilla, in a way similar to IRSNB M.2329.

Because the two specimens differ in a series of minor morphological features (for example the width of the right maxilla between the antorbital notch and the largest dorsal infraorbital foramen, the aspect of the anterodorsal surface of the left nasal, the shape of the lateral surface of the postorbital process of the frontal, and the degree of concavity of the posterior surface of the exoccipital), and considering also their possibly different geological age, as well as their relatively fragmentary state of preservation, they are provisionally kept in separate taxa. That said, the aforementioned new interpretation of the bones of the facial region of the lectotype of *T. antwerpiensis* leads to a number of fundamental changes in the codings of this taxon in the character-taxon matrix (see below).

#### Phylogeny

The main goal of our phylogenetic analysis is to test for the phylogenetic affinities of *Thalassocetus*, based on the new morphological interpretation of its neurocranium as provided above. A more in-depth investigation of relationships within Physeteroidea and of physeteroids with the other main odontocete clades is beyond the scopes of this work. Taking into account the herein morphological reinterpretation of *Thalassocetus antwerpiensis*, seven changes were made for the codings of the latter in the character-taxon matrix published by Collareta *et al.* (2019), namely: 1) character 3 was changed from “?” to “1&2”, since a supracranial basin was identified in *T. antwerpiensis*, although it is not possible to exclude the possibility that it might extend onto the whole dorsal surface of the rostrum; 2) since the right premaxilla is no longer identified on the cranium, character 13 was changed from “1” to “?”; 3) with the lack of a sagittal crest, character 14 was changed from “1” to “0”; 4) the identification of one nasal bone changed character 19 from “2” to “1”; 5) the truncated right maxilla could not allow any supposition on its posterior extent, and character 21 was changed from “1” to “?”; 6) for character 26 the anteroposterior extent of the temporal fossa was assessed to be longer or approximately the same length as the distance between antorbital process of the maxilla and anterior wall of the temporal fossa (changed from “?” to “1&2”); and 7) character 30 dealing with the occipital shield was corrected from “1” to “1&2” because the shield draws an angle between 60 and 90° with the reconstructed long axis of the rostrum and it has a flat surface. For the other, unchanged codings of characters see the matrix in the Appendix 2.

With these corrections for *T. antwerpiensis* and the addition of the new specimen IRSNB M.2329, the heuristic search resulted in 72 most parsimonious trees with 144 steps, a consistency index (CI) of 0.542, and a retention index (RI) of 0.735. The strict consensus tree is shown in Figure 9 with bootstrap support values. It is important to note that, as in previous physeteroid phylogenies, bootstrap values are generally

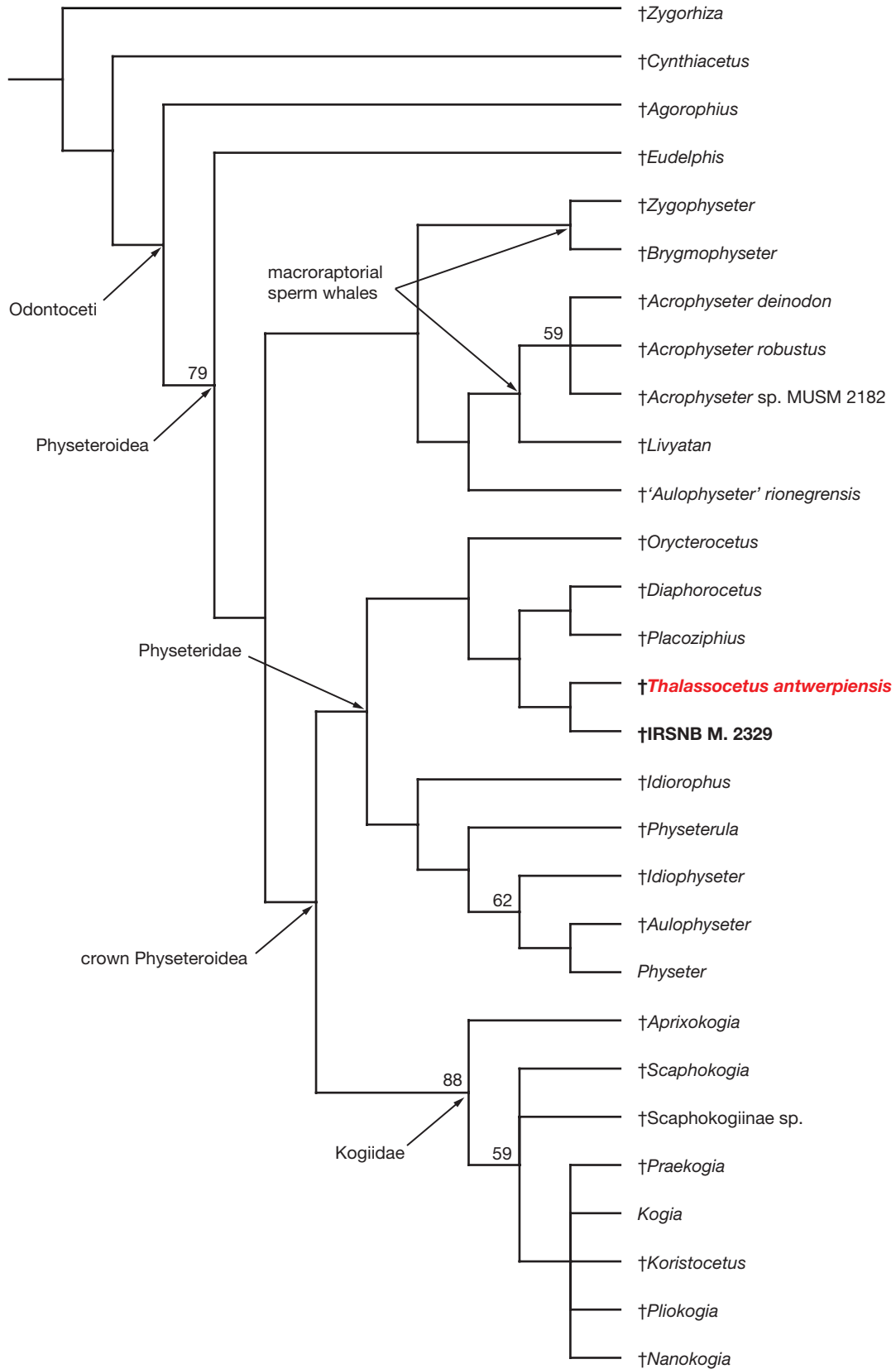


FIG. 9. — Strict consensus of 72 most parsimonious trees resulting from the heuristic search applied to a modified version of the character-taxon matrix of Collareta *et al.* (2019). Bootstrap values higher than 50 are indicated. The consensus tree shows the cranium **IRSNB M.2329** as a sister-group of *Thalassocetus antwerpiensis* Abel, 1905 (IRSNB M.525) within the family Physeteridae. † for extinct taxa.

low (often under 50) for most nodes in all major physeteroid clades, including Physeteridae. Only Kogiidae gets a significantly higher value (which is relevant for the discussion of the status of *Thalassocetus*, our main point of interest, see below). Therefore, relationships as obtained here have to be considered with caution. More complete specimens will allow for the addition of new characters, which may ultimately lead to a stronger support for the main nodes of the physeteroid tree.

Differing from the strict consensus tree of Collareta *et al.* (2019), our analysis recovers *Eudelphis* du Bus, 1872 as sister-group of a clade including macroraptorial physeteroid genera (i.e., *Acrophyseter* Lambert, Bianucci & Muizon, 2008, *Brygmophyseter* Barnes in Kimura, Hasegawa & Barnes, 2006, *Livyatan* Lambert, Bianucci, Post, Muizon, Salas-Gismondi, Urbina & Reumer, 2010, and *Zygophyseter* Bianucci & Landini, 2006) and '*Aulophyseter*' rionegrensis Gondar, 1974 + the crown Physeteroidea (Fig. 9). Among the latter, the family Physeteridae is rearranged in two clades (see below), whereas relationships within the family Kogiidae are less resolved. *Thalassocetus* is no longer inside the Kogiidae, being instead found inside the Physeteridae (defined here by three characters: temporal fossa approximately as long as the distance between the antorbital process of the maxilla and the anterior wall of the temporal fossa; number of mandibular teeth >14, unknown in *Thalassocetus*; and dorsal process of the periotic anteroposteriorly shorter, but dorsally extended beyond the medial margin of the internal acoustic meatus, unknown in *Thalassocetus*, reversion), as the sister-group of the new specimen IRSNB M.2329 (sharing two characters: maximum width of skull <40 cm, reversion, and right premaxillary foramen distinctly anterior to the level of the antorbital notch, reversion), in a clade also including *Diaphorocetus* Ameghino, 1894, *Orycterocetus*, and *Placoziphius* Van Beneden, 1869 (defined by three characters: three large foramina in the area of the right antorbital notch and posteriorly, reversion; right premaxillary foramen slightly anterior to the level of the antorbital notch, reversion; and postorbital process of the frontal much ventrally extended, with a vertical length of the process equal to or greater than the horizontal length of the orbit).

## DISCUSSION AND CONCLUSION

The discovery of a well-preserved small physeteroid cranium (IRSNB M.2329) from the late Miocene of Antwerp (north of Belgium) offers a new perspective on the interpretation of morphological features in the supracranial basin for more fragmentarily known members of this superfamily. Indeed, this juvenile individual retains most of its cranial sutures open. Removable bony elements provide unique insights into the shape and arrangement of the multiple thin bony plates making the floor of the supracranial basin, as part of these plates are hidden by overlying bones in adult physeteroid specimens (e.g. Lambert *et al.* 2017: fig. 18), even more so than on the anteroposteriorly telescoped cranium of other odontocetes (Roston & Roth 2019). Strong morphological similarities with the lectotype of *Thalassocetus antwerpiensis*

allow for a reinterpretation of a series of morphological features from the facial region of the latter. By correcting a series of codings in our character-taxon matrix a sister-group phylogenetic relationship between the two specimens is recovered, supporting the attribution of IRSNB M.2329 to the genus *Thalassocetus*. Furthermore, the two taxa fall in the family Physeteridae, forming with *Placoziphius* and *Diaphorocetus* the sister-group of *Orycterocetus*. *Thalassocetus* is thus removed here from its basal position in the family Kogiidae. The absence of kogiid-like periotics (with a typical, plate-like posterior process; e.g. Muizon 1984; Velez-Juarbe *et al.* 2016) in the large collection of Neogene physeteroid ear bones from the North Sea at the IRSNB (M.B., O.L., pers. obs.) is in line with this major change in *Thalassocetus*' family attribution. As outlined above, the cranium IRSNB M.2329 shares more similarities with *Orycterocetus*, *Placoziphius*, and *T. antwerpiensis* than with any of the other members of the superfamily Physeteroidea, especially regarding the supracranial basin and its components, the posterior part of the maxillae and premaxillae, and the supraorbital region. The changes made in the character-taxon matrix resulted in a new topology for the family Physeteridae, but decreased the phylogenetic resolution among the different taxa of Kogiidae.

This work sheds light on the challenging identification of bones making the supracranial basin, especially in the area of the sagittal crest, of Kogiidae and, more generally, the highly modified nasal bones of physeteroids. It may thus prove informative to reassess the morphology of this cranial region in early kogiids and other, closely related small physeteroids, in the light of the new anatomical interpretations of *T. antwerpiensis*. Future work could help resolving the phylogenetic relationships of Kogiidae. For example, the small physeterid *Placoziphius duboisi* Van Beneden, 1869 shares derived characters with *Kogia* spp., like a premaxilla that is narrower than the maxilla on the rostrum. Interestingly, before its reassessment by Lambert (2008) the lectotype of *T. antwerpiensis* was proposed to belong to *P. duboisi*, due to shared morphological features with an Austrian specimen referred to the latter species (Kazár 2002; Stotzing specimen). Although later noted differences between the type material of *T. antwerpiensis* and *P. duboisi* do not only concern anatomical features of the supracranial basin (Lambert 2008), the present reinterpretation of the anatomy and family-level attribution of *T. antwerpiensis* should be followed by a revision of the Stotzing specimen, unfortunately currently held in a private collection.

More complete specimens may also prove crucial to investigate the evolution of the rostrum, dentition, and ear bones at the transition between stem and crown physeteroids, and more specifically for the largely unknown emergence of kogiids. Indeed, now that the early to middle Miocene *Thalassocetus* is revised as a physeterid, the geologically oldest kogiid fossils date back to the Tortonian (early late Miocene; Velez-Juarbe *et al.* 2015; Collareta *et al.* 2020; Benites-Palomino *et al.* 2020), further extending the ghost lineage separating the divergence date between kogiids and physeterids (estimated around the late Chattian to Aquitanian, latest Oligocene to earliest Miocene; Steeman *et al.* 2009; McGowen *et al.* 2009,

2020) and the first records of fossil kogiids. A biogeographic consequence of this revised attribution of *Thalassocetus* is that the oldest kogiid remains (dated from the Tortonian) are found in the eastern Pacific (Panama and Peru), supporting the hypothesis that the origin of the family could be found in that region. However, the earliest branching kogiid, *Aprixokogia*, has a North Atlantic origin (Whitmore & Kaltenbach 2008). Furthermore, the ghost lineage mentioned above points to a major gap in our knowledge of the early history of the family. We anticipate that the discovery and description of better-preserved skeletons for previously named small physeteroid taxa, as well as new taxa (for example from less extensively prospected areas of the Southern Hemisphere), will help closing this more than 9 million year-long temporal gap, either through the identification of previously unrecognized early kogiids or/and through the reassessment of the taxonomic attribution (as stem physeteroids) of species currently identified as early physeterids. In this context, it is worth noting that relationships between stem physeteroids and early physeterids appear highly volatile in recent phylogenies (e.g. Velez-Juarbe *et al.* 2015; Lambert *et al.* 2017; Collareta *et al.* 2017a, 2019; Paolucci *et al.* 2020; Benites-Palomino *et al.* 2020; this work).

### Acknowledgements

The core of this study was made by A.A. during a Master 1 internship at the IRSNB, between May and June 2019, under the supervision of O.L. We would like to warmly thank L. Dufraing for having generously donated the cranium IRSNB M.2329 to the IRSNB, A. Collareta for providing necessary files for the phylogenetic analysis, C. de Muizon for his many constructive comments on a preliminary version of this work, and A. Collareta and an anonymous reviewer for their detailed reviews, which greatly improved the content of this article. We also thank A. Benites-Palomino, G. Bianucci, D. J. Bohaska, S. Bruaux, C. Cousin, A. Folie, C. Lefèvre, J. G. Mead, C. de Muizon, O. Pauwels, N. D. Pyenson, A. Rol, R. Salas-Gismondi, and R. Varas-Malca for providing access to specimens under their care.

### REFERENCES

- ABEL O. 1905. — Les Odontocètes du Boldérien (Miocène supérieur) des environs d'Anvers. *Mémoires du Musée Royal d'Histoire Naturelle de Belgique* 3: 1-155.
- BARNES L. G. 1973. — *Praekogia cedrosensis*, a new genus and species of fossil pygmy sperm whale from Isla Cedros, Baja California, Mexico. *Contributions in Science, Natural History Museum of Los Angeles County* 247: 1-20.
- BENITES-PALOMINO A., VÉLEZ-JUARBE J., SALAS-GISMONDI R. & URBINA M. 2020. — *Scaphokogia totajpe*, sp. nov., a new bulky-faced pygmy sperm whale (Kogiidae) from the late Miocene of Peru. *Journal of Vertebrate Paleontology* 39: e1728538. <https://doi.org/10.1080/02724634.2019.1728538>
- BIANUCCI G. & LANDINI W. 2006. — Killer sperm whale: a new basal physeteroid (Mammalia, Cetacea) from the Late Miocene of Italy. *Zoological Journal of the Linnean Society* 148: 103-131. <https://doi.org/10.1111/j.1096-3642.2006.00228.x>
- BIANUCCI G., SORCE B., STORAI T. & LANDINI W. 2010. — Killing in the Pliocene: shark attack on a dolphin from Italy. *Palaeontology* 53 (2): 457-470. <https://doi.org/10.1111/j.1475-4983.2010.00945.x>
- BOSSOLAERS M., HERMAN J., HOEDEMAEKERS K., LAMBERT O., MARQUET R. & WOUTERS K. 2004. — A temporary exposure of the Late Miocene Deurne Sand Member in Antwerpen (Flanders, Belgium). *Geologica Belgica* 7 (1-2): 27-39.
- BRISSEN M.-J. 1762. — *Regnum Animale in classes IX distributum, sine synopsis methodica*. Theodorum Haak, Paris, 296 p. <https://www.biodiversitylibrary.org/page/28278568>
- CALDWELL D. K. & CALDWELL M. C. 1989. — Pygmy sperm whale *Kogia breviceps* (de Blainville, 1838): Dwarf sperm whale *Kogia simus* Owen, 1866, in RIDGWAY S. H. & HARRISON R. (eds), *Handbook of marine mammals, vol. 4: River dolphins and the larger toothed whales*. Academic Press, London: 235-260.
- COLLARETA A., LAMBERT O., DE MUIZON C., URBINA M. & BIANUCCI G. 2017a. — *Koristocetus pescei* gen. et sp. nov., a diminutive sperm whale (Cetacea: Odontoceti: Kogiidae) from the late Miocene of Peru. *Fossil Record* 20: 259-278. <https://doi.org/10.5194/fr-20-259-2017>
- COLLARETA A., LAMBERT O., LANDINI W., DI CELMA C., MALINVERNO E., VARAS-MALCA R., URBINA M. & BIANUCCI G. 2017b. — Did the giant extinct shark *Carcharocles megalodon* target small prey? Bite marks on marine mammal remains from the late Miocene of Peru. *Palaeogeography, Palaeoclimatology, Palaeoecology* 469: 84-91. <https://doi.org/10.1016/j.palaeo.2017.01.001>
- COLLARETA A., FULGOSI F. C. & BIANUCCI G. 2019. — A new kogiid sperm whale from northern Italy supports psychrospheric conditions in the early Pliocene Mediterranean Sea. *Acta Palaeontologica Polonica* 64 (3): 609-626. <https://doi.org/10.4202/app.00578.2018>
- COLLARETA A., LAMBERT O., DE MUIZON C., BENITES PALOMINO A. M., URBINA M. & BIANUCCI G. 2020. — A new physeteroid from the late Miocene of Peru expands the diversity of extinct dwarf and pygmy sperm whales (Cetacea: Odontoceti: Kogiidae). *Comptes Rendus Palevol* 19 (5): 79-100. <https://doi.org/10.5852/cr-palevol2020v19a5>
- CRANFORD T. W., AMUNDIN M. & NORRIS K. S. 1996. — Functional morphology and homology in the Odontocete nasal complex: implications for sound generation. *Journal of Morphology* 228: 223-285. [https://doi.org/10.1002/\(SICI\)1097-4687\(199606\)228:3<::AID-JMOR1&gt;3.0.CO;2-3](https://doi.org/10.1002/(SICI)1097-4687(199606)228:3<::AID-JMOR1&gt;3.0.CO;2-3)
- FLOWER W. H. 1867a. — Description of the skeleton of *Inia geoffrensis* and the skull of *Pontoporia blainvillii*, with remarks on the systematic position of these animals in the Order Cetacea. *Transactions of the Zoological Society of London* 6: 87-116. <https://doi.org/10.1111/j.1096-3642.1867.tb00572.x>
- FLOWER W. H. 1867b. — On the osteology of the cachalot or sperm-whale (*Physeter macrocephalus*). *Transactions of the Zoological Society of London* 6: 309-372. <https://doi.org/10.1111/j.1096-3642.1868.tb00580.x>
- FORDYCE R. E. & MUIZON C. DE 2001. — Evolutionary history of cetaceans: a review, in MAZIN J.-M. & BUFFRÉNIL V. de (eds), *Secondary adaptation of tetrapods to life in water*. Verlag Dr. Friedrich Pfeil, München: 169-233.
- GOOLAERTS S., DE CEUSTER J., MOLLEN F. H., GIJSEN B., BOSSOLAERS M., LAMBERT O., UCHMAN A., VAN HERCK M., ADRIAENS R., HOUTHUYS R., LOUWYÉ S., BRUNEEL Y., ELSÉN J. & HOEDEMAEKERS K. 2020. — The upper Miocene Deurne Member of the Diest Formation revisited: unexpected results from the study of a large temporary outcrop near Antwerp International Airport, Belgium. *Geologica Belgica* 23: 219-252. <https://doi.org/10.20341/gb.2020.011<>
- GRAY J. E. 1821. — On the natural arrangement of vertebrate animals. *London Medical Repository* 15: 296-310.
- HEYNING J. E. 1989. — Comparative facial anatomy of beaked whales (Ziphiidae) and a systematic revision among the families of extant Odontoceti. *Contributions in Science, Natural History Museum of Los Angeles County* 405: 1-64.

- HOEDEMAEKERS K. & DUFRAING L. 2015. — Elasmobranchii in de ontsluiting aan de luchthaven te Borsbeek (prov. Antwerpen, België). *Afzettingen van de Werkgroep voor Tertiaire en Kwartaire Geologie* 36 (1): 12-19.
- HUGGENBERGER S., ANDRÉ M. & OELSCHLÄGER H. H. 2016. — The nose of the sperm whale: overviews of functional design, structural homologies and evolution. *Journal of the Marine Biological Association of the United Kingdom* 96 (4): 783-806. <https://doi.org/10.1017/S0025315414001118>
- KALLAL R. J., GODFREY S. J. & ORTNER D. 2012. — Bone reactions on a Pliocene cetacean rib indicate short-term survival of predation event. *International Journal of Osteoarchaeology* 22 (3): 253-260.
- KAZÁR E. 2002. — Revised phylogeny of the Physeteridae (Mammalia: Cetacea) in the light of *Placoziphius* Van Beneden, 1869 and *Aulophyseter* Kellogg, 1927. *Bulletin de L'Institut Royal des Sciences Naturelles de Belgique, Sciences de la Terre* 72: 151-170.
- KELLOGG R. 1965. — Fossil marine mammals from the Miocene Calvert Formation of Maryland and Virginia. The Miocene Calvert sperm whale *Orycterocetus*. *Bulletin of the United States National Museum* 247 (2): 47-63.
- LAMBERT O. 2005. — Systematics and phylogeny of the fossil beaked whales *Ziphirostrum* du Bus, 1868 and *Choneziphius* Duvernoy, 1851 (Cetacea, Odontoceti), from the Neogene of Antwerp (North of Belgium). *Geodiversitas* 27: 443-497.
- LAMBERT O. 2008. — Sperm whales from the Miocene of the North Sea: a re-appraisal. *Bulletin de L'Institut Royal des Sciences Naturelles de Belgique, Sciences de la Terre* 78: 277-316.
- LAMBERT O., BIANUCCI G. & MUIZON C. DE 2017. — Macroraptorial sperm whales (Cetacea, Odontoceti, Physeteroidea) from the Miocene of Peru. *Zoological Journal of the Linnean Society* 179 (2): 404-474.
- LOUWYÉ S. 2005. — The Early and Middle Miocene transgression at the southern border of the North Sea Basin (northern Belgium). *Geological Journal* 40: 441-456. <https://doi.org/10.1002/gj.1021>
- LOUWYÉ S., DE SCHEPPER S., LAGA P. & VANDENBERGHE N. 2007. — The Upper Miocene of the southern North Sea Basin (northern Belgium): a palaeoenvironmental and stratigraphical reconstruction using dinoflagellate cysts. *Geological Magazine* 144 (1): 33-52. <https://doi.org/10.1017/S0016756806002627>
- LOUWYÉ S., MARQUET R., BOSSELAERS M. & LAMBERT O. 2010. — Stratigraphy of an early-middle Miocene sequence near Antwerp in Northern Belgium (Southern North Sea Basin). *Geologica Belgica* 13 (3): 269-284.
- MCGOWEN M. R., SPAULDING M. & GATESY J. 2009. — Divergence date estimation and a comprehensive molecular tree of extant cetaceans. *Molecular Phylogenetics and Evolution* 53 (3): 891-906. <https://doi.org/10.1016/j.ympev.2009.08.018>
- MCGOWEN M. R., TSAGKOGEOGA G., ÁLVAREZ-CARRETERO S., DOS REIS M., STRUEBIG M., DEAVILLE R., JEPSON P. D., JARMAN S., POLANOWSKI A. & MORIN P. A. 2020. — Phylogenomic resolution of the cetacean tree of life using target sequence capture. *Systematic Biology* 69 (3): 479-501. <https://doi.org/10.1093/sysbio/sy2068>
- MUIZON C. DE 1984. — Les vertébrés de la Formation Pisco (Pérou). Deuxième partie: Les Odontocètes (Cetacea, Mammalia) du Pliocène inférieur de Sud-Sacaco. *Travaux de l'Institut Français d'Etudes Andines* 27: 1-188.
- MUIZON C. DE 1991. — A new Ziphiidae (Cetacea) from the Early Miocene of Washington State (USA) and phylogenetic analysis of the major groups of odontocetes. *Bulletin du Muséum national d'Histoire naturelle, Paris* 12: 279-326.
- PAOLUCCI F., BUONO M. R., FERNÁNDEZ M. S., MARX F. G. & CUITIÑO J. I. 2020. — *Diaphorocetus poucheti* (Cetacea, Odontoceti, Physeteroidea) from Patagonia, Argentina: one of the earliest sperm whales. *Journal of Systematic Palaeontology* 18 (4): 335-355. <https://doi.org/10.1080/14772019.2019.1605544>
- RICE D. W. 1989. — Sperm whale *Physeter macrocephalus* Linnaeus, 1758, in RIDGWAY S. H. & HARRISON R. (eds), *Handbook of marine mammals, vol. 4: River dolphins and the larger toothed whales*. Academic Press, London 177-233.
- ROSS G. J. B. 1984. — The smaller cetaceans of the south east coast of southern Africa. *Annals of the Cape Provincial Museums of Natural History* 15 (2): 173-410.
- ROSTON R. A. & ROTH V. L. 2019. — Cetacean skull telescoping brings evolution of cranial sutures into focus. *The Anatomical Record* 302 (7): 1055-1073. <https://doi.org/10.1002/ar.24079>
- STEEHAN M. E., HEBBSGAARD M. B., FORDYCE R. E., HO S. Y. W., RABOSKY D. L., NIELSEN R., RAHBK C., GLENNER H., SØRENSEN M. V. & WILLERSLEV E. 2009. — Radiation of extant cetaceans driven by restructuring of the oceans. *Systematic Biology* 58 (6): 573-585. <https://doi.org/10.1093/sysbio/syp060>
- SWOFFORD D. L. 2001. — *PAUP\*. Phylogenetic analysis using parsimony (\*and other methods). Version 4b10*. Sinauer Associates, Sunderland, Massachusetts. <https://paup.phylosolutions.com/>
- UHEN M. D. 2008. — New protocetid whales from Alabama and Mississippi, and a new cetacean clade, Pelagiceti. *Journal of Vertebrate Paleontology* 28 (3): 589-593. [https://doi.org/10.1671/0272-4634\(2008\)28\[589:NPWFAA\]2.0.CO;2](https://doi.org/10.1671/0272-4634(2008)28[589:NPWFAA]2.0.CO;2)
- VÉLEZ-JUARBE J., WOOD A. R., DE GRACIA C. & HENDY A. J. W. 2015. — Evolutionary patterns among living and fossil kogiid sperm whales: Evidence from the Neogene of Central America. *PLoS ONE* 10 (4): e0123909. <https://doi.org/10.1371/journal.pone.0123909>
- VÉLEZ-JUARBE J., WOOD A. R. & PIMIENTO C. 2016. — Pygmy sperm whales (Odontoceti, Kogiidae) from the Pliocene of Florida and North Carolina. *Journal of Vertebrate Paleontology* 36: e1135806. <https://doi.org/10.1080/02724634.2016.1135806>
- WHITMORE F. C. JR. & KALTENBACH J. A. 2008. — Neogene Cetacea of the Lee Creek Phosphate Mine, North Carolina. *Virginia Museum of Natural History Special Publication* 14: 181-269.

Submitted on 21 April 2020;  
accepted on 8 July 2020;  
published on 11 October 2021.

## APPENDICES

APPENDIX 1. — List of characters used in the cladistic analysis. Characters taken from Collareta *et al.* (2019).

1. Rostrum length: 0, rostrum elongated, ratio between rostrum length and skull width  $>1.2$ ; 1, ratio between 1.2 and 0.95; 2, short rostrum, ratio  $<0.95$ .
2. Maxillae, premaxillae and vomer, all reaching the tip of the rostrum which is not formed only by the premaxillae: 0, absent; 1, present.
3. Supracranial basin of the skull: 0, absent; 1, present but anteriorly short; 2, extended onto the whole dorsal surface of the rostrum.
4. Dorsal exposure of the maxilla on the rostrum: 0, exposure limited to less than half the rostrum length; 1, maxilla exposed on more than half the length of the rostrum, narrower than the premaxilla at some levels; 2, maxilla exposed on the whole length of the rostrum, wider than the premaxilla all along.
5. Constriction of premaxilla anterior to antorbital notch followed by anterior expansion: 0, absent, suture maxilla-premaxilla on the rostrum roughly anteriorly directed; 1, present, suture maxilla-premaxilla distinctly anterolaterally directed.
6. Upper tooth row: 0, deep alveoli; 1, alveoli shallow or absent.
7. Premaxillary teeth: 0, present; 1, absent. This character cannot be coded for taxa lacking distinct upper alveoli.
8. Maximum width of skull (postorbital or bizygomatic width): 0,  $<40$  cm; 1, from 40 to (but excluding) 60 cm; 2, from 60 to (but excluding) 100 cm; 3, 100 cm and more.
9. Antorbital notch: 0, absent; 1, present; 2, transformed into a very narrow slit.
10. Right antorbital notch: 0, outside the supracranial basin; 1, inside the supracranial basin.
11. Number and size of dorsal infraorbital foramina, in the area of the right antorbital notch and posteriorly: 0, small to moderate size foramina, at least three-four; 1, three large foramina; 2, two large foramina; 3, one large foramen (maxillary incisure).
12. Right premaxilla: 0, posteriorly extended as the left premaxilla; 1, more posteriorly extended than the left premaxilla.
13. Right premaxilla: 0, not widened posteriorly; 1, posterior extremity of the right premaxilla laterally widened, occupying at least one third of the width of the supracranial basin, mostly on the right side.
14. Presence of a sagittal crest: 0, absent; 1, present as a shelf covered by the pointed right premaxilla.
15. Left premaxillary foramen very small or absent: 0, absent (i.e. foramen present and not reduced); 1, present.
16. Increase in size of the right premaxillary foramen: 0, absent, ratio between width of foramen and width of premaxilla at that level 0.20; 1, present, ratio  $>0.20$ .
17. Anteroposterior level of right premaxillary foramen: 0, distinctly anterior to antorbital notch; 1, slightly anterior to antorbital notch; 2, same level or posterior to antorbital notch.
18. Asymmetry of the bony nares: 0, absent or reduced; 1, strong, left bony naris significantly larger than right naris.
19. Lack of nasals: 0, both nasals present; 1, one nasal absent; 2, both nasals absent.
20. Widening of the supracranial basin on the right side: 0, absent; 1, present, basin overhangs the right orbit.
21. Right maxilla reaching the sagittal plane of the skull on the posterior wall of the supracranial basin: 0, absent; 1, present.
22. Fusion of lacrimal and jugal: 0, absent; 1, present.
23. Projection of the lacrimal-jugal between frontal and maxilla: 0, short or absent; 1, long.
24. Dorsoventral level of the antorbital process of the frontal: 0, higher than the lateral margin of rostrum base; 1, at approximately the same level; 2, considerably lower.
25. Frontal-maxilla suture, with skull in lateral view: 0, forming an angle  $<15^\circ$  from the axis of the rostrum; 1,  $15\text{--}35^\circ$ ; 2,  $>35^\circ$ .
26. Temporal fossa: 0, anteroposteriorly longer than distance between preorbital process of the maxilla and anterior wall of temporal fossa; 1, approximately same length; 2, distinctly shorter.
27. Zygomatic process of squamosal in lateral view: 0, 'L'-shaped with dorsal margin ventrally bending in its posterior portion; 1, triangular, with dorsal margin dorsally bending in its posterior portion.
28. Postglenoid process of the squamosal: 0, significantly ventrally longer than post-tympanic process; 1, roughly same ventral extent as post-tympanic process.
29. In lateral view of the skull, wide notch posterior to the postglenoid process of the squamosal for the enlarged posterior process of the tympanic: 0, absent; 1, present but only partially developed, paraoccipital concavity moderately excavated; 2, present and well developed, paraoccipital concavity transformed in a wide and deep notch.
30. Occipital shield: 0, convex and forming an angle of about  $40^\circ$  from the axis of the rostrum; 1, as state 0 with an angle of about  $60^\circ$ ; 2, flat or concave forming an angle of about  $90^\circ$ ; 3, flat or concave forming an angle distinctly greater than  $90^\circ$ .
31. Falciform process of the squamosal: 0, contacting the corresponding pterygoid; 1, forming a thin plate not contacting the pterygoid; 2, reduced to a simple peg or absent.

32. Anterior bullar facet of the periotic: 0, very anteroposteriorly elongated; 1, reduced; 2, absent or very small.
33. Posterior extension of the posterior process of the periotic parallel to the general plane of the bone and not ventrally orientated: 0, absent; 1, present.
34. Accessory ossicle of the tympanic bulla: 0, absent or small; 1, enlarged and partially fused with the anterior process of the periotic.
35. Involucrum of the tympanic bulla with an evident central concavity, visible in ventral and medial views, due to the marked pachyostosis of its anterior and posterior portion: 0, absent; 1, present.
36. Size of teeth (greatest transverse diameter of root expressed as percentage of the maximum width of skull): 0, <5 %; 1, >5 %. Considering the strong heterodonty in *Cynthiacetus* and *Zygorhiza* this character is restricted to single-rooted teeth.
37. Loss of dental enamel: 0, absent; 1, present.
38. Number of mandibular teeth: 0, 11; 1, 12–14; 2, >14.
39. Labiolingual compression of the posterior lower teeth (portion out of the alveolus): 0, strong; 1, weak or absent.
40. Ventral position of the mandibular condyle: 0, absent, well-developed angular process; 1, present, angular process low or absent.
41. Anteroposterior level of last upper alveolus or posterior end of vestigial alveolar groove: 0, posterior to antorbital process; 1, at level of antorbital notch or slightly anterior; 2, distinctly anterior to the notch.
42. Lateral margin of the supraorbital process of the maxilla: 0, dorsoventrally thin; 1, significantly dorsoventrally thickened, making a subvertical wall.
43. Postorbital process of the frontal: 0, moderately posteroventrally extended; 1, much ventrally extended (vertical length of process equal or greater than horizontal length of orbit), with a correspondingly low position of the zygomatic process of the squamosal.
44. Height of temporal fossa: 0, dorsal margin at top of skull or somewhat lower; 1, much lower, temporal fossa making less than half the skull height.
45. Contact between jugal and zygomatic process of squamosal: 0, anteroposteriorly long contact; 1, proportionally short, more rounded contact; 2, no contact. In specimens with no jugal preserved, the contact surface can sometimes be observed on the zygomatic process (e.g., *Orycterocetus crocodilinus* USNM 22926).
46. Length of the zygomatic process of the squamosal (horizontal length from anterior tip to posterior margin of squamosal): 0, ratio between length of the process and bizygomatic width of skull >0.35; 1, ratio <0.35.
47. Medial to tympanosquamosal recess, deep and rectilinear narrow groove in ventral surface of squamosal, from spiny process area to temporal fossa: 0, absent or shallow and poorly delineated; 1, present.
48. Dorsal process of the periotic: 0, dorsally extended and anteroposteriorly long; 1, anteroposteriorly shorter, but dorsally extended beyond the medial margin of the internal acoustic meatus; 2, dorsally short.
49. Posteromedial outline of the pars cochlearis in dorsal view: 0, angular; 1, flattened, barely convex, and roughly continuous with posterior margin of dorsal process.
50. Curvature of the mandible in lateral view: 0, absent or reduced, ventral margin roughly rectilinear or rising moderately anterodorsally; 1, conspicuous, ventral margin distinctly convex rising both posterodorsally and anterodorsally; 2, present, ventral margin concave.
51. Symphyseal angle on the mandibles: 0, <35°; 1, 35–55°; 2, >55°.
52. Lateral margin of atlas: 0, roughly rectilinear or laterally concave; 1, convex, with laterally pointed transverse process at mid-height of the bone. Not applicable to *Kogia* (single block of cervical vertebrae).
53. Notch in the anterior margin of the basihyal: 0, wide and shallow notch; 1, narrow and deep notch; 2, no notch, rectilinear or convex anterior margin.

APPENDIX 2. — Character–taxon matrix used in the cladistic analysis. Modified from Collareta *et al.* (2019): [https://doi.org/10.5852/cr-palevol2021v20a39\\_s1](https://doi.org/10.5852/cr-palevol2021v20a39_s1)